Vortex structure of excitation fields in a supercooled glass-forming liquid and its relationship with relaxations

Y. J. Lü,[*] H. R. Qin, and C. C. Guo

School of Physics, Beijing Institute of Technology, Beijing 100081, People's Republic of China

In the framework of the dynamic facilitation model, a glass former is structured with local cooperative excitations in space and time when approaching the glass transition, which is closely related to dynamic relaxations. We investigate the structure of excitation fields in supercooled $Cu_{50}Zr_{50}$ glass former, and reveal that the excitation fields feature the vortexlike structure beyond the well-known stringlike excitations. The vortex is developed from the stringlike excitations and frequently annihilates via the interactions between vortex and antivortex. The region favored by vortices exhibits percolationlike morphology. We find that the probability distributions of vortex core number are characterized by the discrete multiple mode, which is very analogous to the quantized mode of the slow-β type relaxation. Furthermore, the relaxation time derived from the formation rate of vortices as well as the corresponding activation energy coincide with the characteristic values of the slow-β relaxation in metallic glasses. Therefore, it is concluded that the vortex excitation is the origin of the slow-β relaxation in dynamic space. We further find that the activation energy and relaxation time associated with individual excitations agree well with the Johari-Goldstein β relaxation. It manifests a more intrinsic structural sign of the Johari-Goldstein β relaxation than the interpretation based on stringlike excitations.

I. INTRODUCTION

Supercooled glass-forming liquids exhibit more complex dynamic behaviors than simple liquids. The structural relaxation (α-relaxation) time is found to diversely increase upon approaching the glass transition for different glass formers. Angell thus classified supercooled liquids into "strong" and "fragile" based on the temperature dependence of structural relaxation or viscosity [1–3]. The strong glass formers refer to the liquids with the Arrhenius-type temperature dependence, and the fragile liquids refer to those with the super-Arrhenius behavior. The divergence of the relaxation time of fragile glass formers is empirically fitted by the Vogel-Fulcher-Tamman law (VFT), $\tau_\alpha = \tau_0 \exp[DT_0/(T - T_0)]$, where the parameter D provides a good measurement of the deviation from the Arrhenius behavior, or fragility [1,4]. The structural relaxation is contributed to the calorimetric glass transition, a process from the supercooled liquid state to the nonequilibrium glass state [5,6]. In the past several decades, extensive experimental and numerical studies have proved the existence of secondary relaxation processes hidden in the structural relaxation through the glass transition [7–11]. The dynamics of glass-forming liquids in fact covers multiple time- and space scales, and its comprehensive understanding is a key issue in glassy physics.

The diversity of relaxation behaviors reflects the dynamic heterogeneity, the spatiotemporal fluctuation of dynamics, which was argued to be a critical-like phenomenon [12,13]. Microscopically, the dynamic heterogeneity manifests the coexistence of immobile and mobile atomic regions. The

mobile dynamics close to T_g was suggested to be dominated by the jump event, a sudden hopping of particles after the long-time vibration around well-defined positions [14,15]. The cage-jump motion of single particles provides a microscopic perspective on the macroscopic dynamics of glassy systems: the cage time (the time interval between two successive jumps) and persistent time (the waiting time before the first jump) scaled by the mean-squared jump length were found to be related to the timescales of structural relaxation and diffusion motion [16]. Furthermore, the coexistence of two dynamic phases associated with the two characteristic timescales were observed in a short timescale, which hints at the microscopic origin of the Stokes-Einstein breakdown in supercooled liquids [17,18]. Despite the attempt based on the single-particle dynamics, the macroscopic dynamics of glass and supercooled liquids is more frequently interpreted as a result of cooperative motions in many theoretical models. Adam and Gibbs have proposed that there are collective particle arrangement regions with a cooperative way in dynamically heterogeneous liquids, the so-called "cooperatively rearranging regions (CRRs)," and the length scale of CRRs grows when approaching the glass transition [19–21]. The idea of CRRs is analogous to the definition of mosaic state within the context of the random first-order transition (RFOT) theory, an ordered microscopic separated state whose length scale grows upon supercooling [22,23]. Computer simulations and experiments have revealed that the shape of CRRs changes from being stringlike in the relatively high-temperature region to being more compact near T_g [24,25]. This change corresponds to a crossover from activated to nonactivated dynamics.

The stringlike cooperative manner is consistent with the representation of dynamic facilitation (DF) theory. Computer

---
*[*]yongjunlv@bit.edu.cn

simulations have suggested that an excitation event tends to facilitate its neighbors to move simultaneously, forming a stringlike morphology [26–28]. In the framework of DF theory, sparse or mobile domains are defined as defects in glass-forming liquids [12,29]. These defects can facilitate the excitation of their neighbors, forming excitation lines or strings that surround immobile regions. The slowdown of structural relaxation upon the glass transition was thus explained as the reduction of excitation concentrations so that the immobile region takes longer time to relax. However, it was argued that the cooperative stringlike excitations were the structural origin of the Johari-Goldstein secondary (β) relaxation [30]. Besides the β-relaxation process, recent experiments and numerical simulations have reported an intermediate timescale relaxation process between α- and β relaxation, the so-called slow-β relaxation, which was similarly attributed to the cooperative excitations [31,32]. These inconsistent explanations based on cooperative excitations imply that understanding multiscale relaxation processes within the framework of the facilitated excitation is still an open question. In this work, we investigate the structure of excitation fields in a metallic glass-forming liquid using molecular-dynamics (MD) simulations. We reveal that the excitation field has well-structured vortices. The probability distribution of vortex number exhibits the multiple hierarchical modes, and it is proved to be the structural origin of the slow-β relaxation process. We further clarify that the individual excitations are responsible for the Johari-Goldstein β relaxation irrespective of its cooperative manner.

II. COMPUTATIONAL METHODS

A. Molecular-dynamics simulations

MD simulations were used to study the dynamics of supercooled $Cu_{50}Zr_{50}$ liquid. A bulk system consisting of $N = 4000$ atoms was relaxed for 2 ns at $T = 1800\,K$ to produce the equilibrium liquid. The system was then quenched in isothermal-isobaric ensemble with a cooling rate of $1 \times 10^{10}\,Ks^{-1}$, i.e., a relaxation of 2 ns per 20 K until the glass transition occurs. The calorimetric glass transition temperature is approximately $T_g = 660\,K$, which is evaluated by the variation of enthalpy with temperature. The trajectories were sampled in the temperature range from 800 to 680 K after a waiting time of $t_w = 100$ ns at each temperature. The atomic interactions were calculated by using the embedded atom method potential [33]. We calculated the overlap between configurations at t_w and $t_w + t$,

$$C(t, t_w) = \frac{1}{N} \sum_{i=1}^{N} \Theta(a - |r_i(t_w + t) - r_i(t_w)|), \quad (1)$$

where $\Theta(x)$ is the Heaviside function and $a = 1.0\,\text{Å}$ [34,35]. The relaxation time $\tau(t_w)$ is obtained by fitting the ensemble average $\langle C(t, t_w) \rangle$ to the Kohlrausch-Williams-Watts law, $A \exp[-(t/\tau)^\beta]$, where β is the stretching exponent. In simulations, 200–300 independent relaxation processes were sampled at each temperature for sufficient statistics. The periodic boundary conditions were employed in the three dimensions and the MD time step was 1 fs.

B. Analysis method for excitation fields

We classify atomic motions in supercooled liquids into two categories: jump and move. A jump means the rapid jump motion of a particle after long-time vibrations in the neighbors' cage, which can be directly confirmed from the squared displacements of individual atoms by MD simulations [36]. Here, using the time coarse-grained position of atoms, $\bar{r}_i(t)$,

$$\bar{\mathbf{r}}_i(t) = \frac{1}{\Delta t} \int_0^{\Delta t} \mathbf{r}_i(t + t')dt', \quad (2)$$

where Δt is the time window, a jump event is identified when the moving distance between two subsequent time windows is larger than the cage size that is defined as three times the Debye-Waller (DW) factor. The DW factor is approximated to the value at the inflection point in the mean-squared displacement curve, positively depending on temperature [36,37]. The time coarse-graining procedure is used to improve the temporal resolution by smoothing the thermal noise. The value of Δt was suggested to have only a small influence on the single-particle dynamics [38]. In general, a small Δt is favored (it should be much smaller than the waiting time between two successive jump events to avoid missing jumps), and on the other hand, the time window should comprise sufficient trajectory points. In the present simulation, the value of $\Delta t = 40$ ps, comprising 80 trajectory points, is used in all the cases, which is allowed to well capture the jump events approaching the glass transition. A jump is defined as an excitation event, and the excitation vector, $\mathbf{j}_i$ for atom i is then given by

$$\mathbf{j}_i(t) = \bar{\mathbf{r}}_i(t + \Delta t) - \bar{\mathbf{r}}_i(t). \quad (3)$$

The excitation vector for caged atoms is approximately zero. All the excitations taking place in an observation time t_{obs} constitute an excitation field. We divide the simulation cell into $M = 28 \times 28 \times 28$ grids, and average the excitation vectors in each grid. Then the excitation field is represented by $\mathbf{J}_k = \sum_{t < t_{\text{obs}}} \sum_{i \in k} \mathbf{j}_i(t)$, where $k = 1, 2, \ldots M$. Here we focus on the vortex analysis of excitation fields. By calculating the curl of the excitation field, the vorticity $\boldsymbol{\omega}$ is given as

$$\omega_x = \frac{\partial J_z}{\partial y} - \frac{\partial J_y}{\partial z}$$
$$\omega_y = \frac{\partial J_x}{\partial z} - \frac{\partial J_z}{\partial x}$$
$$\omega_z = \frac{\partial J_y}{\partial x} - \frac{\partial J_x}{\partial y}. \quad (4)$$

To analyze the number of vortex as well as its distribution, the vortex core should be identified. We use the Q criterion to find vortex cores in excitation fields [39]. The parameter Q is defined as

$$Q = \tfrac{1}{2}(\|\Omega^2\| - \|S^2\|), \quad (5)$$

where Ω is the vorticity tensor, $\Omega_{ij} = 0.5(\partial J_i/\partial r_j + \partial J_j/\partial r_i)$, and S is the rate-of-strain tensor, $S_{ij} = 0.5(\partial J_i/\partial r_j - \partial J_j/\partial r_i)$, $(i, j = x, y, z)$. A vortex core is identified when $Q > 0.1$ in this work. The observation time t_{obs} is set as 1.6 ns, which covers 40 time windows. This value can ensure the observation of stable excitation fields.
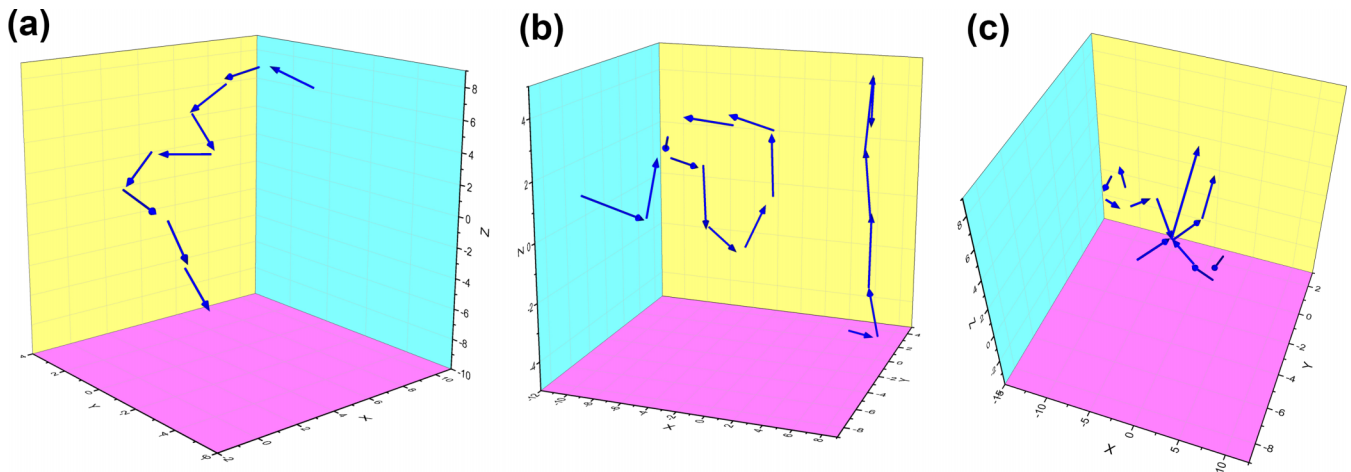
FIG. 1. Typical structures of collective excitation events. (a) Stringlike excitation; (b) looplike excitation; and (c) collision of stringlike excitations.

III. RESULTS AND DISCUSSION

A. Structure of excitation fields in supercooled $Cu_{50}Zr_{50}$ liquid

The contributions of "jump" and "move" motions to the relaxation dynamics differentially depend on temperature. In the equilibrium liquid state and low supercooling region, the jump and move rates, the event number observed per unit time, are very close. They were believed to jointly contribute to the structural relaxation. The jump events were found to be strongly suppressed but their time-spatial correlation significantly increases when the temperature is reduced below the critical temperature of mode-coupling theory, T_c [14,26]. In this region, jump excitations were suggested to be associated with the secondary relaxation. Our analyses of excitation fields in this work are performed mainly in the temperature range of T_c–T_g (approximately 800–660 K for $Cu_{50}Zr_{50}$ glass former) to explore the relation between the structure of excitation fields and the secondary relaxation.

There are three types of excitation events, depending on the time-space correlation. The first one is the independent excitation, which occurs randomly in the observation time. This excitation is massively observed in high-temperature regime and becomes rare upon approaching the glass transition. The second one is the successive excitation of the same atom, and it is time correlated. The third one is the space-correlated excitation: an excitation facilitates its neighbors to excite cooperatively as described in the DF theory. The last two excitation events dominate the excitation field near the glass transition. We have demonstrated that jumps at high temperatures are mostly activated thermally but those in the relatively low-temperature regime are driven by stress which is related to the existence of sparse zones as described in the free-volume model [40,41].

In contrast to the random distribution of independent excitations at high temperatures, the space-time correlated excitations are often assembled into excitation clusters with special spatial structure, which becomes more pronounced when approaching T_g. Figure 1 shows three typical cluster structures. Stringlike cluster is the most common one in them, as shown in Fig. 1(a). It is noted that a long string is usually not assembled in several successive time windows; more

possibly, its growth pauses for a while and then continues. The stringlike structural arrangements have been widely confirmed in various glassy systems and been regarded as the intrinsic feature of CRRs in the intermediate supercooling regime [24,25,30]. In few cases, the stringlike excitation is developed into a loop, as shown in Fig. 1(b). The loop size ranges from three to ten single excitations and does not show the temperature dependence. Once the excitation loop forms, the extension of strings is terminated. Some strings are found to collide and birth new strings, as shown in Fig. 1(c), which can change the extension direction of stringlike excitations.

Beyond the local structure of excitations in space and time as displayed in Fig. 1, we extend the observation time to 40 time windows (1.6 ns) and find that some turbulent regions connected by strings exist in excitation fields, as shown in Fig. 2(a). These turbulent regions actually are originated from strings or loops, and they frequently come forth and disappear but never die. Like the stringlike excitation, the turbulent excitation is one of intrinsic structures in excitation fields. The turbulent excitation regions are analogous to the percolationlike CRRs predicted by the thermodynamic model based on RFOT [20], where the compromise between the cost of localizing an atom, TS_c (S_c is the configurational entropy) and the interfacial free-energy gain determines the CRR shape [24,42]. The stable shape was suggested to become more compact at low temperatures, which is consistent with the present results that more turbulent regions form near T_g.

Here we focus on the structure of excitation flows. The turbulent excitation domains display the vortex characteristic to some extent. To check the vortex distribution, we search the underlying vortex cores using the Q criterion as described in Sec. II B. Figure 2(b) shows a typical turbulent domain and the red balls indicate the positions of vortex cores (the ball size depends on the value of Q parameter). It is clear that the turbulent domain is structured with vortices. The large turbulent domain is composed of multiple excitation loops and strings, displaying pronounced vortex structure. The excitation field thus can be described as a vortex field. Figure 3 shows the contour of the x component of vorticity as well as its evolution with time at $T = 680$ K. A variety of vorticity regions with different signs are distributed in vortex fields, and the positive
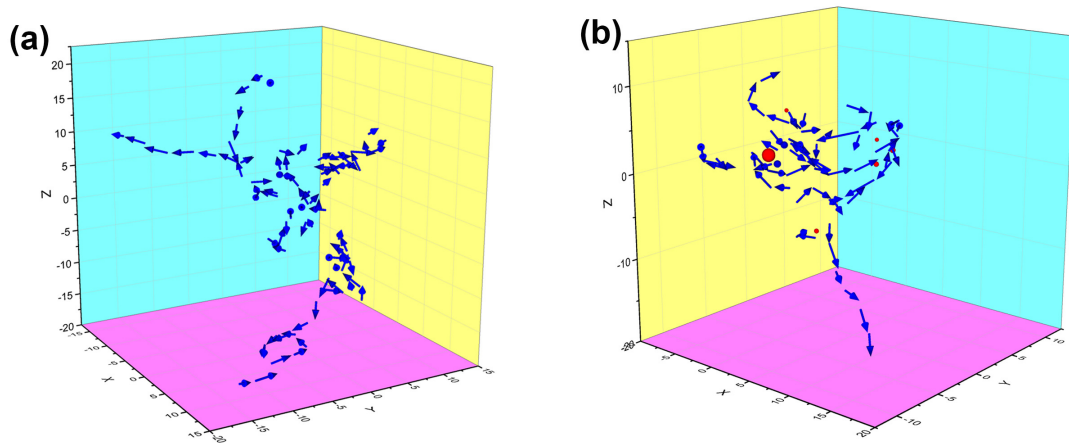
FIG. 2. Vortex structures in excitation fields. (a) An excitation field observed in 1.6 ns at $T = 680$ K. (b) A representation of typical vortex topology. The red balls indicate the locations of vortex cores identified by the Q criterion and the ball size is scaled by the Q value.

vorticity domains (vortex) are generally coupled with negative ones (antivortex), as exhibited in Fig. 3(a). Such vortex structure is not static; the positive and negative vorticity regions can interact with each other, resulting in the annihilation of vortices [Figs. 3(b)–3(e)]. Meanwhile, new vortices are created elsewhere, and ultimately the stable field characterized by the constant formation rate of vortices, the number of vortices formed per unit time, is expected. Our simulations confirm that the stable vortex field is available in the observation time of $t_{obs} = 1.6$ ns due to approximately constant formation rate given longer t_{obs}. Despite the homogeneous distribution of vortices in time, the spatial distribution shows a preference. We mark all the spatial regions that vortex cores have visited over a long observation time of 5 ns, as shown in Fig. 4. The regions favored by vortices look like the percolationlike CRRs; the intervortex zones indicate the inactive regions that cannot effectively trigger the formation of vortices.

B. Relationship between vortex and relaxation dynamics

1. Relaxation characteristics in supercooled Cu₅₀Zr₅₀ liquid

The excitation events are closely related to the relaxation dynamics. The DF theory predicts that the structural relaxation is determined by the size of excitation regions. The inactive regions relax relying on the excitation strings surrounding them: the smaller the spatial extension of excitations, the slower the inactive regions relax. Numerical simulations have claimed that the length-scale fluctuation of excitation strings is in accord with the structural relaxation [21]. However, we also note the argument that the string-like excitation is the structural origin of the Johari-Goldstein β relaxation [28,43]. Obviously, the relation between the relaxation dynamics and the excitation structure remains a controversial issue. Here we aim to reveal the role of excitations with different structures in relaxations.
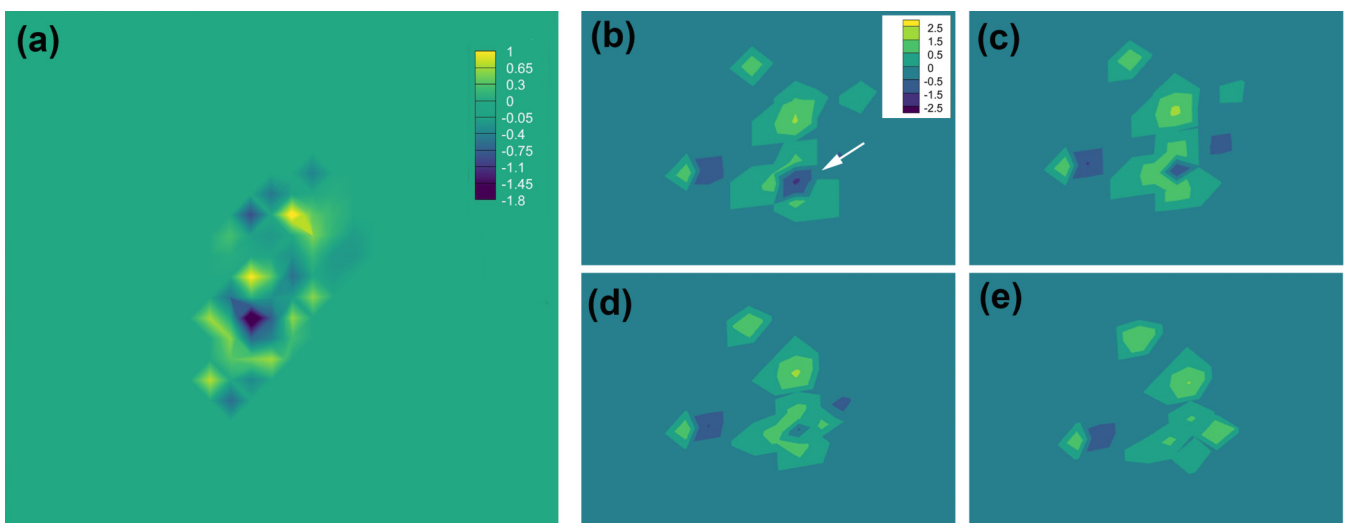

FIG. 3. Vorticity contour of excitation fields along the x direction. (a) A slice of the vorticity contour diagram. It shows the coupling of vortices and antivortices; (b)–(e) show the annihilation of an antivortex indicated by the white arrow. The color is scaled by the vorticity along the x direction, ω_x, defined in Eq. (4).
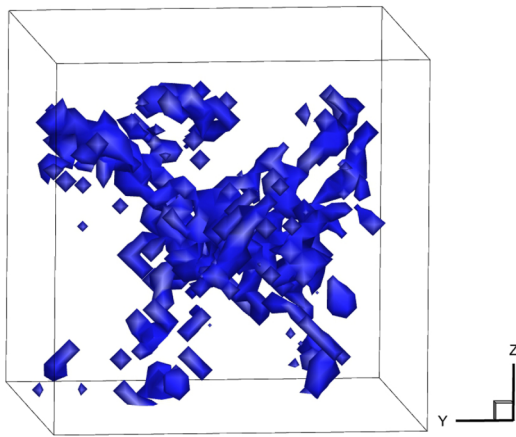
FIG. 4. Spatial distribution of vortex cores in the observation time of 5 ns at $T = 680$ K.

We used the configurational overlap function [Eq. (1)] to measure the relaxation time. Our previous studies have revealed that the distributions of relaxation time, which are sampled from massive independent trajectories close to T_g, do not follow the single mode, but show multiple discrete Gaussian-type mode, namely quantized relaxation mode [44]. This relaxation behavior resembles the multiple anelastic relaxation phenomenon observed in Al-based metallic glasses [45,46], and is also analogous to the multiple decays in the enthalpy recovery processes of a Au-based metallic glass [31]. In the present work, we further check the distribution of relaxation time up to high-temperature region, and find that distinct quantized relaxation effect appears when $T <$ 800 K, approximately T_c. Figure 5 shows the distributions of relaxation time with decreasing temperature, where more than 200 independent relaxation processes were sampled at each temperature. The relaxation time distribution shifts to the slow dynamic region in a whole as accompanied by more slow relaxation modes are activated when approaching T_g. The fastest relaxation mode has the highest visiting probability and then the probability decreases approximately following a stretched exponential function, $\sim \exp[-(t_i/\tau)^\beta]$ towards slower modes, where t_i is the relaxation time corresponding to the peak value of the ith mode and τ is the average relaxation time. Our studies have reported that the probability distribution depends on the waiting time or aging time at a given temperature [42]. As the supercooled melt is relaxed to the equilibrium state, the exponent β decays to zero, suggesting the identical visiting probability for various relaxation modes. From the viewpoint of the energy landscape theory, each relaxation mode maps a minimum in the potential energy landscape (PEL). The distributions of these PEL minima are hierarchical and the relaxation time actually reflects the average effect of various minima. When the supercooled liquid is relaxed into equilibrium states, the difference in quantity between various minima is eliminated and the configurational entropy reaches the maximum.
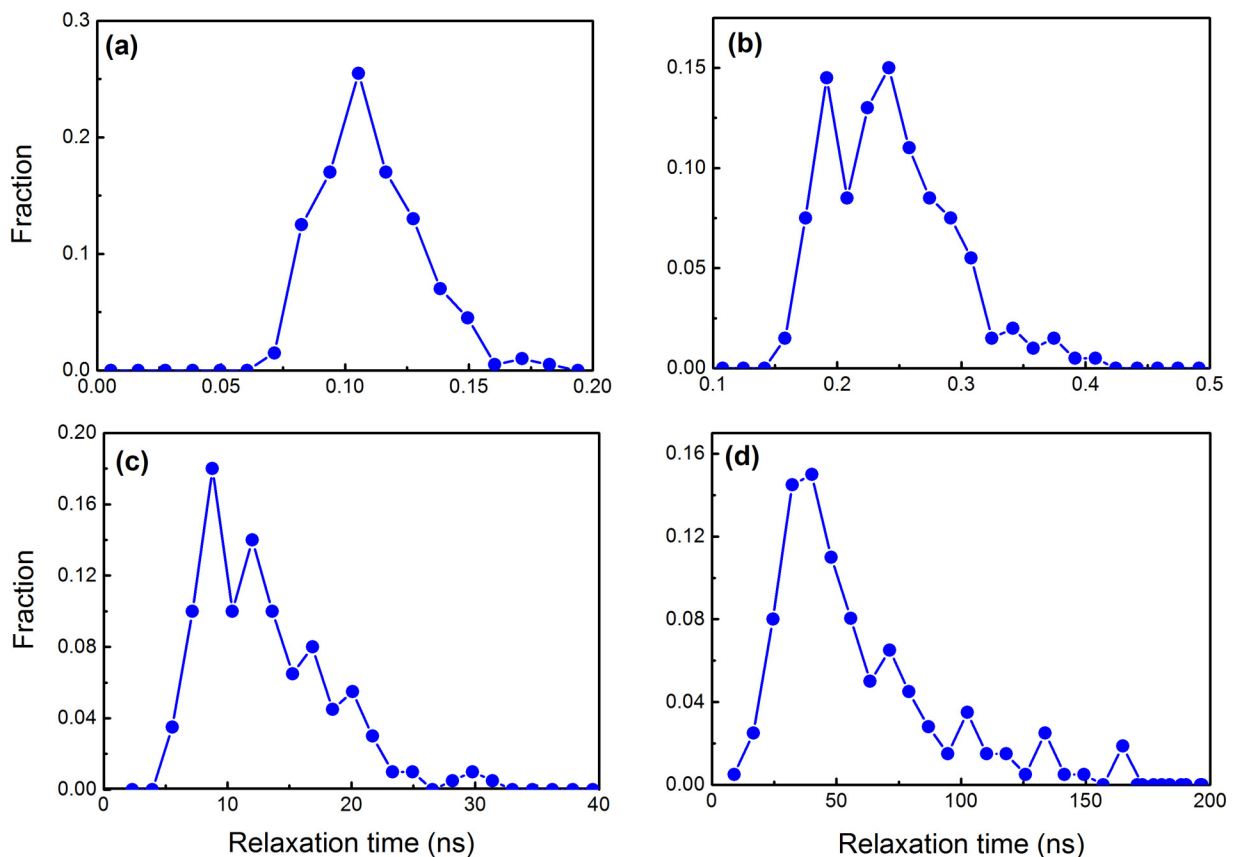

FIG. 5. Multimode distributions of relaxation time. (a) $T = 800$ K, (b) $T = 780$ K (c) $T = 720$ K, and (d) $T = 680$ K. Each distribution is achieved via 200–300 independent relaxation processes after $t_w = 100$ ns.
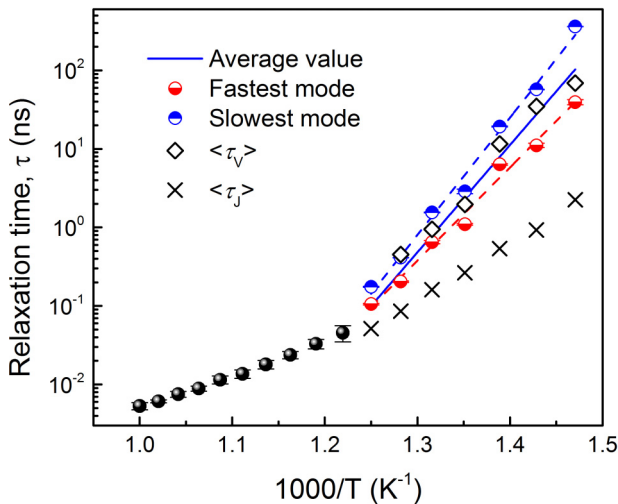
FIG. 6. Average relaxation time as a function of the inverse of temperature. The down and upper half open symbols denote the average relaxation times corresponding to the fastest and the slowest relaxation modes, respectively. The open diamond symbols are the relaxation time, $\langle \tau_V \rangle$ derived from the formation rate of vortices, and the cross symbols are relaxation time, $\langle \tau_J \rangle$ for individual excitations. The solid line is the average value over all the relaxation modes. The dashed lines are fits to the Arrhenius law for the fastest and slowest mode. The solid symbols are the average relaxation time in 800–1000 K.

Based on the quantized relaxation dynamics, we calculate three average relaxation times: the average relaxation time for the fastest mode, the slowest mode, and the overall relaxation time. Figure 6 shows the relaxation time as a function of the inverse of temperature. To have a clear view of the change of temperature dependence, the average values ranging from 1000 to 800 K are also provided. The most remarkable characteristic is that all the three average relaxation times obey the Arrhenius increase with decreasing temperature down to T_g. However, they strongly deviate from the extrapolation of the high-temperature Arrhenius behavior of relaxation time. The deviation cannot well be described by the VFT. We use the Arrhenius law, $\tau = A \exp(\Delta E / k_B T)$, to fit the relaxation time in the low-temperature region independently and obtain the effective activation energies, $\Delta E = 285.8$, 226.6, and 251.3 kJ mol^{-1} for the slowest, fastest modes, and the overall case, respectively. Obviously, the activation energy rises as the relaxation shifts to higher (slower) modes. A primary question we have to face is how to define the present relaxation behavior. The activation energies of the quantized relaxation mode are much larger than the value of the well-known Johari-Goldstein β relaxation, 142.7 kJ mol^{-1} ($\sim 26RT_g$, where R is the gas constant) [47,48], and thus they are not characterized by the Johari-Goldstein β relaxation. On the other hand, the present relaxation processes do not show the divergence when approaching the calorimetric glass transition temperature, and therefore, they differ from the structural relaxation that is responsible for glass transition. We note that the stress relaxation experiments have found that the secondary relaxation of metallic glasses below T_g is decoupled into a fast and a slow mode [8]. The slow mode follows the Arrhenius law with the

activation energy of 51.7RT_g [8], which is much larger than the Johari-Goldstein β-relaxation process. The similar slow Arrhenius-type relaxation processes were also reported in enthalpy recovery experiments [31], and they were classified into a new branch of β relaxation featuring slower timescale, namely slow-β relaxation [31]. In view of the glass transition temperature in simulations ($T_g \approx 660$ K), the present activation energy is approximately in the range of $41.3 \sim 52.1RT_g$, which coincides with the slow-β relaxation mentioned above. Therefore, the quantized relaxation is identified as the slow-β relaxation process.

The quantized relaxation behavior would be influenced by aging. We have proved that increasing t_w activates more slow relaxation modes, and meanwhile the relaxation spectrum shifts to the long-time regime, leading to approximately sublinear increase of the average relaxation time [44]. Here we further examine the influence of aging on the relaxation time spectra over a wider temperature range above T_g at $t_w = 1$ ns. The relaxation time of the slowest and the fastest mode as well as the overall value are found to still follow the Arrhenius law but the activated energies are decreased to 254.0, 205.2, and 243.2 kJ mol^{-1}, respectively [36]. It is clear that long aging process slows down the relaxation behavior and the activation becomes more difficult with decreasing temperature, which may be connected to more complex structural rearrangement required by the low-temperature relaxation. In the following section, we will give an explanation of slow-β relaxation presented in this work from the view of the structure of excitation fields.

2. Vortex-determined relaxation

To check the relation between the quantized relaxation behavior and the vortex structure of excitation fields, we analyze the distribution of the vortex core number covering 200 independent excitation fields observed in a time interval of 1.6 ns each. Figures 7(a)–7(c) show the probability distributions at different temperature. Similar to the quantized relaxation presented in Fig. 6, the formation of vortices in excitation fields follows a multiple-mode manner. With decreasing temperature, the size of vortices, namely the number of excitations involved in a vortex, is reduced companied by the emergence of more vortex modes. More importantly, the visiting probabilities increase with shifting to the higher-order modes (more vortex cores), which is against the distribution of relaxation time that decreases toward high-order modes. In each mode, we find that the distribution of Q values follows a nontrial distribution: although the vortex core number seems to have an approximately exponential decrease with increasing Q [Fig. 7(d)], the decay is actually accompanied by weak fluctuations [inset in Fig. 7(d)]. It suggests that there are some characteristic vortex structures favored by excitation fields.

The formation rate of vortices, υ_c, reflects the formation ability of vortices in excitation fields analogous to the nucleation rate in crystallization. Figure 8 shows the average formation rate of vortices as a function of temperature (left axis). It decreases following an Arrhenius law with temperature, and the effective activation energy of vortices, DE_V, is 237.5 kJ mol^{-1}. This value is close to the average activation energy of slow-β relaxation shown in Fig. 6. Given a
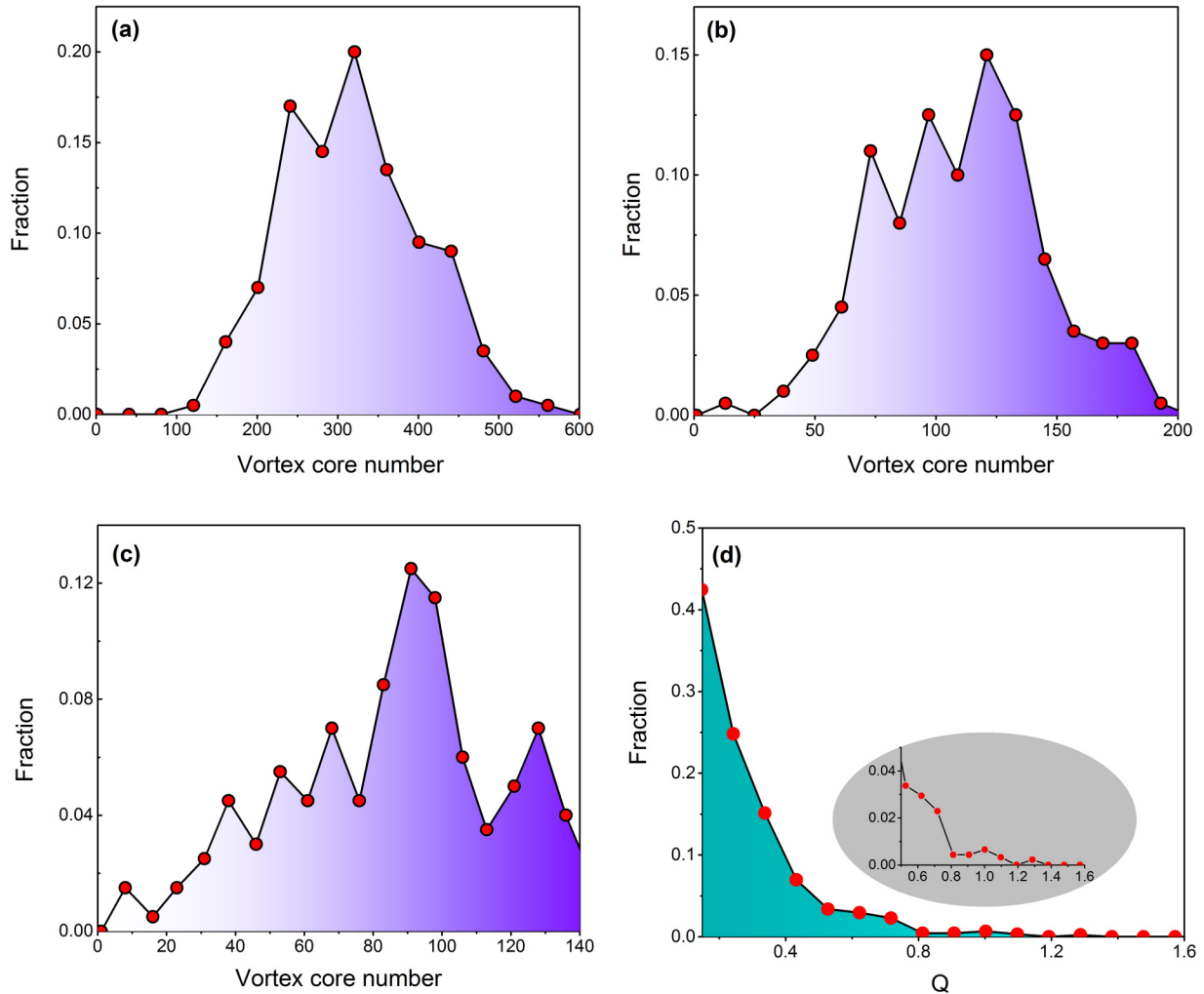
FIG. 7. Statistic distributions of vortex core number at $t_w = 100$ ns. (a) $T = 780$ K, (b) $T = 740$ K, and (c) $T = 680$ K. (d) shows the probability distribution of Q values at 680 K. The inset is the magnification to illustrate the fluctuation of Q values.

relaxation process associated with the formation of vortices, the time quantity $\langle \tau_V \rangle = \upsilon_c^{-1}$ is expected to serve as the timescale featuring the relaxation of vortex structure. The open diamond symbols in Fig. 6 show the values of $\langle \tau_V \rangle$, which well match the average relaxation time of the slow-β process. Considering these agreements, we confirm that the formation of vortices is responsible for the slow-β relaxation process; in other words, the vortex is the origin of slow-β relaxation in dynamic space. In the case of $t_w = 1$ ns, the activation energy of vortices is reduced to 210.6 kJ mol^{-1} [36]. It qualitatively agrees with the decrease in the activation energy that is directly deduced from the relaxation time as t_w decreases to 1 ns. Therefore, the influences of aging on the relaxation time and the formation of vortices are in line with each other. In addition, by comparing Fig. 5 with Fig. 7, the favored excitation field is characterized by faster relaxation mode, and meanwhile, has more vortices. This correspondence is consistent with the prediction of DF theory.

As for the stringlike structure, its role in relaxation dynamics seems more complex. The correlated length of stringlike motions was argued to grow accompanied by the slowdown of structural relaxation, and on the other hand, the timescale

was found to coincide with the Johari-Goldstein β relaxation [29,30]. If putting this contradiction aside, we wonder whether the individual excitations differ with collective modes, in other words, whether the individual excitation events involved in a vortex are easier than that in a string. We define the excitation rate as $\upsilon_j = N_j / N_0 t_{obs}$, where N_j is the excitation number in observation time t_{obs}, and N_0 is the total number of atoms. Figure 8 shows that the excitation rate has the Arrhenius-type decrease when approaching T_g (right axis), suggesting that the mechanism of individual excitations associated with string and vortex has no significant difference. The activation energy of individual excitations, DE_J is approximately 140.2 kJ mol^{-1}, which well agrees with the reported value of the Johari-Goldstein β relaxation in metallic glasses (142.7 kJ mol^{-1}). In the case of $t_w = 1$ ns, the activation energy is reduced to 133.4 kJ mol^{-1} [36]. On the other hand, if the individual excitation is indeed related to the β relaxation, the time defined by the excitation rate $\langle \tau_J \rangle = \upsilon_j^{-1}$ should feature the β-relaxation process like the slow-β relaxation associated with vortex discussed above. Figure 6 presents the results of $\langle \tau_J \rangle$ (cross symbols) superimposed on the relaxation time derived from Eq. (1). The relaxation time associated with the individual excitation is significantly faster than the
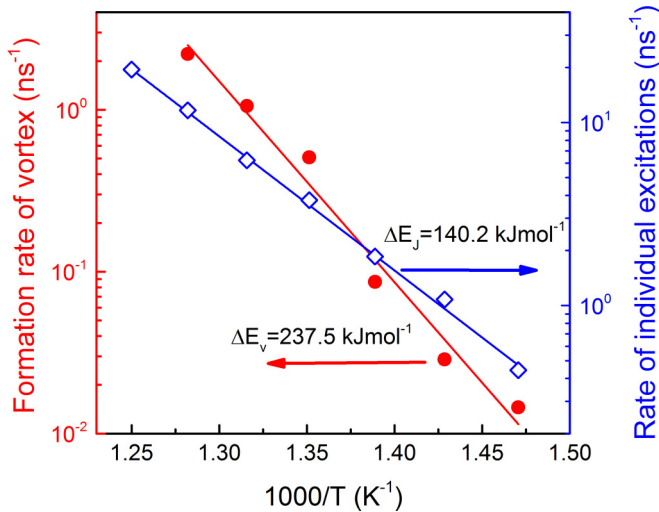
FIG. 8. Formation rate of vortex cores and the individual excitation rate as a function of the inverse of temperature. The solid lines are fits to the Arrhenius law, yielding that the activation energies of vortex and individual excitations are 237.5 and 140.2 kJ mol^{-1}, respectively.

slow-β relaxation and smoothly joins in the high-temperature relaxation. This characteristic agrees with the description of Johari-Goldstein β relaxation [7]. Therefore, we argue that it is the individual excitation rather than the stringlike excitation that contributes to the Johari-Goldstein β relaxation. Since the stringlike excitation is the dominant morphology of excitations in intermediate supercooling region, it looks like the structural signature of β-relaxation events; in fact, the present results clarify that the individual excitation plays a more intrinsic role in it. Synchrotron x-ray investigations have demonstrated that the β relaxation in ZrCuNiAl glass originates from short-range atomic arrangement within the nearest-neighboring distance [49]. The spatial scale is consistent with the individual excitation and validates the present simulation results.

The stringlike excitations serve as the precursor to trigger the formation of vortices. Some stringlike excitations are found to grow into loops or helical chains, and ultimately develop into vortices by collision and coalescence of neighboring strings. Therefore, the excitation field can be described as a mixture of vortexlike and stringlike structures. It is difficult to accurately distinguish stringlike excitations in it. Here we assume that the grid with $Q < 0$ is shared by a string, and the total number of grids with $Q < 0$ thus can roughly reflect the size of strings in the excitation field. By using the formation rate of strings, the size of strings per unit time, the activation energy of strings is expected to be calculated. We assume that the temperature dependence of activation energy of strings follows the Arrhenius law, and then the estimated activation energy is 190.1 kJ mol^{-1} [36]. This value is much larger than the conventional Johari-Goldstein β relaxation but smaller than the slow-β relaxation. It is close to the value corresponding to the fastest mode of the slow-β relaxation. These numeric comparisons suggest that the stringlike excitation may represent a limit case of vortex excitations with open structure.

Finally, we check the influence of finite-size effects on the relaxation dynamics and the structure of excitation fields. We used a larger system with $N = 16\,384$ to analyze the rates of vortex and individual excitations at $t_w = 1$ ns following the similar simulation procedure mentioned above. The results do not show any distinct effects due to the finite size of simulation cells [36]. The relaxation time is also in accord with the results for $N = 4000$ within the error allowed. Thus the system under consideration here ($N = 4000$) is large enough to describe the characteristics of excitation fields as well as the relaxation behavior. In fact, in a time window, the average number of vortices is less than 50 and the excitation events are less than 200 in the present temperature range. These amounts are quite small compared to the system size. It should be noted that the correlation length associated with excitation zones tends to increase as the system is supercooled across glass transition. The influences of the finite size on excitation rate and relaxation time need to be checked carefully, in particular below the glass transition.

IV. CONCLUSIONS

We study the structure of excitation fields of supercooled $Cu_{50}Zr_{50}$ glass-forming liquid and its relationship with dynamic relaxation using MD simulations. We reveal that there is intrinsic vortex structure in excitation fields beyond the previous knowledge of stringlike excitations. The vortices are coupled with the antivortices and their interaction induces the annihilation of vortices. We find that the number of vortices displays the multiple-mode distribution at a given temperature close to the glass transition. The visiting probabilities increase as approaching high-order modes. On the other hand, we show that slow-β relaxation processes that are slowed down following the Arrhenius law toward the glass transition exhibit the multiple-mode distribution similar to the case of vortex. The relaxation time associated with vortex, which is evaluated by the formation rate of vortices, is found to be well in line with the average value of the slow-β relaxation. Moreover, the activation energy of vortices coincides with the slow-β relaxation. These facts verify that vortex in excitation fields is the origin of slow-β relaxation processes. We further show that the relaxation time and the activation energy of individual excitation events agree with the Johari-Goldstein β relaxation, which suggests that, more intrinsically, the individual excitations are responsible for the Johari-Goldstein β relaxation rather than stringlike ones. This work provides a perspective on excitation fields and promotes our understanding of the relationship between dynamic structure and relaxation.

[1] C. A. Angell, Relaxation in liquids, polymers and plastic crystals — strong/fragile patterns and problems, J. Non-Cryst. Solids **131**, 13 (1991).

[2] C. A. Angell, Formation of glasses from liquids and biopolymers, Science **267**, 1924 (1995).

[3] P. G. Debenedetti and F. H. Stillinger, Supercooled liquids and the glass transition, Nature (London) **410**, 259 (2001).

[4] L. Beithier and G. Biroli, Theoretical perspective on the glass transition and amorphous materials, Rev. Mod. Phys. **83**, 587 (2011).

[5] L.-M. Wang, V. Velikov, and C. A. Angell, Direct determination of kinetic fragility indices of glassforming liquids by differential scanning calorimetry: Kinetic versus thermodynamic fragilities, J. Chem. Phys. **117**, 10184 (2002).

[6] J. E. K. Schawe, Vitrification in a wide cooling rate range: The relations between cooling rate, relaxation time, transition width, and fragility, J. Chem. Phys. **141**, 184905 (2014).

[7] H. B. Yu, W. H. Wang, and K. Samwer, The β relaxation in metallic glasses: An overview, Mater. Today **16**, 183 (2013).

[8] P. Luo, P. Wen, H. Y. Bai, B. Ruta, and W. H. Wang, Relaxation Decoupling in Metallic Glasses at Low Temperatures, Phys. Rev. Lett. **118**, 225901 (2017).

[9] N. B. Olsen, T. Christensen, and J. C. Dyre, β relaxation of nonpolymeric liquids close to the glass transition, Phys. Rev. E **62**, 4435 (2000).

[10] B. Ruta, E. Pineda, and Z. Evenson, Relaxation processes and physical aging in metallic glasses, J. Phys.: Condens. Matter **29**, 503002 (2017).

[11] F. A. de Melo Marques, R. Angelini, E. Zaccarelli, B. Farago, B. Ruta, G. Ruocco, and B. Ruzicka, Structural and microscopic relaxations in a colloidal glass, Soft Matter **11**, 466 (2015).

[12] M. D. Ediger, Spatially heterogeneous dynamics in supercooled liquids, Annu. Rev. Phys. Chem. **51**, 99 (2000).

[13] H. Tanaka, T. Kawasaki, H. Shintani, and K. Watanabe, Critical-like behaviour of glass-forming liquids, Nat. Mater. **9**, 324 (2010).

[14] J. Helfferich, F. Ziebert, S. Frey, H. Meyer, J. Farago, A. Blumen, and J. Baschnagel, Continuous-time random-walk approach to supercooled liquids. I. Different definitions of particle jumps and their consequences, Phys. Rev. E **89**, 042603 (2014).

[15] R. Pastore, A. Coniglio, and M. P. Ciamarra, From cage-jump motion to macroscopic diffusion in supercooled liquids, Soft Matter **10**, 5724 (2014).

[16] R. Pastore, T. Kikutsuji, F. Rusciano, N. Matubayasi, K. Kim, and F. Greco, Breakdown of the Stokes–Einstein relation in supercooled liquids: A cage-jump perspective, J. Chem. Phys. **155**, 114503 (2021).

[17] M. P. Ciamarra, R. Pastore, and A. Coniglio, Particle jumps in structural glasses, Soft Matter **12**, 358 (2016).

[18] R. Pastore, A. Coniglio, and M. P. Ciamarra, Dynamic phase coexistence in glass–forming liquids, Sci. Rep. **5**, 11770 (2015).

[19] G. Adam and J. H. Gibbs, On the temperature dependence of cooperative relaxation properties in glass-forming liquids, J. Chem. Phys. **43**, 139 (1965).

[20] G. Biroli and C. Cammarota, Fluctuations and Shape of Cooperative Rearranging Regions in Glass-Forming Liquids, Phys. Rev. X **7**, 011011 (2017).

[21] H. Zhang, C. Zhong, J. F. Douglas, X. D. Wang, Q. P. Cao, D. X. Zhang, and J. Z. Jiang, Role of string-like collective atomic motion on diffusion and structural relaxation in glass forming Cu-Zr alloys, J. Chem. Phys. **142**, 164506 (2015).

[22] T. R. Kirkpatrick, D. Thirumalai, and P. G. Wolynes, Scaling concepts for the dynamics of viscous liquids near an ideal glassy state, Phys. Rev. A **40**, 1045 (1989).

[23] J.-P. Bouchaud and G. Biroli, On the Adam-Gibbs-Kirkpatrick-Thirumalai-Wolynes scenario for the viscosity increase in glasses, J. Chem. Phys. **121**, 7347 (2004).

[24] J. D. Stevenson, J. Schmalian, and P. G. Wolynes, The shapes of cooperatively rearranging regions in glass-forming liquids, Nat. Phys. **2**, 268 (2006).

[25] S. Gokhale, R. Ganapathy, K. H. Nagamanasa, and A. K. Sood, Localized Excitations and the Morphology of Cooperatively Rearranging Regions in a Colloidal Glass-Forming Liquid, Phys. Rev. Lett. **116**, 068305 (2016).

[26] Y. J. Lü and W. H. Wang, Single-particle dynamics near the glass transition of a metallic glass, Phys. Rev. E **94**, 062611 (2016).

[27] A. S. Keys, L. O. Hedges, J. P. Garrahan, S. C. Glotzer, and D. Chandler, Excitations Are Localized and Relaxation Is Hierarchical in Glass-Forming Liquids, Phys. Rev. X **1**, 021013 (2011).

[28] S. Swayamjyoti, J. F. Löffler, and P. M. Derlet, Local structural excitations in model glasses, Phys. Rev B **89**, 224201 (2014).

[29] J. P. Garrahan and D. Chandler, Geometrical Explanation and Scaling of Dynamical Heterogeneities in Glass Forming Systems, Phys. Rev. Lett. **89**, 035704 (2002).

[30] H. B. Yu, R. Richert, and K. Samwer, Structural rearrangements governing Johari-Goldstein relaxations in metallic glasses, Sci. Adv. **3**, e1701577 (2017).

[31] I. Gallino, D. Cangialosi, Z. Evenson, L. Schmitt, S. Hechler, M. Stolpe, and B. Ruta, Hierarchical aging pathways and reversible fragile-to-strong transition upon annealing of a metallic glass former, Acta Mater. **144**, 400 (2018).

[32] X. Monnier, D. Cangialosi, B. Ruta, R. Busch, and I. Gallino, Vitrification decoupling from α-relaxation in a metallic glass, Sci. Adv. **6**, eaay1454 (2020).

[33] M. I. Mendelev, M. J. Kramer, R. T. Ott, D. J. Sordelet, D. Yagodin, and P. Popel, Development of suitable interatomic potentials for simulation of liquid and amorphous Cu–Zr alloys, Philos. Mag. **89**, 967 (2009).

[34] N. Lačević, F. W. Starr, T. B. Schrøder, and S. C. Glotzer, Spatially heterogeneous dynamics investigated via a time-dependent four-point density correlation function, J. Chem. Phys. **119**, 7372 (2003).

[35] Y. C. Hu, P. F. Guan, Q. Wang, Y. Yang, H. Y. Bai, and W. H. Wang, Pressure effects on structure and dynamics of metallic glass-forming liquid, J. Chem. Phys. **146**, 024507 (2017).

[36] See Supplemental Material at http://link.aps.org/supplemental/10.1103/PhysRevB.104.224103 for the technical details about the single-particle dynamics, the simulation results on the effect of aging on relaxation and excitations, activation energy of stringlike excitations, as well as the finite-size effects.

[37] L. Larini, A. Ottochian, C. de Michele, and D. Leporini, Universal scaling between structural relaxation and vibrational dynamics in glass-forming liquids and polymers, Nat. Phys. **4**, 42 (2008).

[38] J. Helerich, Ph.D. thesis, University of Freiburg, Freiburg, 2015 (available at https://freidok.uni-freiburg.de/data/9985).

[39] J. C. R. Hunt, A. A. Wray, and P. Moin, Eddies, streams, and convergence zones in turbulent flows, in *Proceeding of the Summer Program in Center for Turbulence Research* (NASA Ames/Stanford University, USA, 1988), pp. 193–208.

[40] Q. L. Bi, Y. J. Lü, and W. H. Wang, Multiscale Relaxation Dynamics in Ultrathin Metallic Glass-Forming Films, Phys. Rev. Lett. **120**, 155501 (2018).

[41] D. Turnbull and M. H. Cohen, Free-volume model of the amorphous phase: Glass transition, J. Chem. Phys. **34**, 120 (1961).

[42] J. D. Stevenson and P. G. Wolynes, A universal origin for secondary relaxations in supercooled liquids and structural glasses, Nat. Phys. **6**, 62 (2010).

[43] S. Karmakar, C. Dasgupta, and S. Sastry, Short-Time Beta Relaxation in Glass-Forming Liquids is Cooperative in Nature, Phys. Rev. Lett. **116**, 085701 (2016).

[44] Y. J. Lü, C. C. Guo, H. S. Huang, J. A. Gao, H. R. Qin, and W. H. Wang, Quantized aging mode in metallic glass-forming liquids, Acta Mater. **211**, 116873 (2021).

[45] M. Atzmon and J. D. Ju, Microscopic description of flow defects and relaxation in metallic glasses, Phys. Rev. E **90**, 042313 (2014).

[46] J. D. Ju, D. Jang, A. Nwankpa, and M. Atzmon, An atomically quantized hierarchy of shear transformation zones in a metallic glass, J. Appl. Phys. **109**, 053522 (2011).

[47] H. B. Yu, W. H. Wang, H. Y. Bai, Y. Wu, and M. W. Chen, Relating activation of shear transformation zones to β relaxations in metallic glasses, Phys. Rev. B **81**, 220201(R) (2010).

[48] L. Hu and Y. Yue, Secondary relaxation in metallic glass formers: Its correlation with the genuine Johari−Goldstein relaxation, J. Phys. Chem. C **113**, 15001 (2009).

[49] Y. H. Liu, T. Fujita, D. P. B. Aji, M. Matsuura, and M. W. Chen, Structural origins of Johari-Goldstein relaxation in a metallic glass, Nat. Commun. **5**, 3238 (2014).